Monthly Notices of the ROYAL ASTRONOMICAL SOCIETY

MNRAS **516,** 4669–4678 (2022) https://doi.org/10.1093/mnras/stac2490
Advance Access publication 2022 September 3

Common envelopes in massive stars II: The distinct roles of hydrogen and helium recombination

Mike Y. M. Lau [1,2,3★] Ryosuke Hirai [1,2] Daniel J. Price [1] and Ilya Mandel [1,2]

[1] *School of Physics and Astronomy, Monash University, Clayton, Victoria 3800, Australia*
[2] *OzGrav – The ARC Centre of Excellence for Gravitational Wave Discovery, Australia*
[3] *Center for Computational Astrophysics, Flatiron Institute, 162 Fifth Avenue, New York, NY 10010, USA*

Accepted 2022 August 27. Received 2022 August 5; in original form 2022 June 13

ABSTRACT

The role of recombination during a common-envelope event has been long debated. Many studies have argued that much of hydrogen recombination energy, which is radiated in relatively cool and optically thin layers, might not thermalize in the envelope. On the other hand, helium recombination contains ≈30 per cent of the total recombination energy, and occurs much deeper in the stellar envelope. We investigate the distinct roles played by hydrogen and helium recombination in a common-envelope interaction experienced by a 12 $M_\odot$ red supergiant donor. We perform adiabatic, 3D hydrodynamical simulations that (i) include hydrogen, helium, and H_2 recombination, (ii) include hydrogen and helium recombination, (iii) include only helium recombination, and (iv) do not include recombination energy. By comparing these simulations, we find that the addition of helium recombination energy alone ejects 30 per cent more envelope mass, and leads to a 16 per cent larger post-plunge-in separation. Under the adiabatic assumption, adding hydrogen recombination energy increases the amount of ejected mass by a further 40 per cent, possibly unbinding the entire envelope, but does not affect the post-plunge separation. Most of the ejecta becomes unbound at relatively high (>70 per cent) degrees of hydrogen ionisation, where the hydrogen recombination energy is likely to expand the envelope instead of being radiated away.

Key words: hydrodynamics – methods: numerical – binaries: close – stars: massive – supergiants.

1 INTRODUCTION

The ability for recombination energy to help eject expanding stellar envelopes was initially explored in the context of planetary nebula formation from single stars (Lucy 1967; Roxburgh 1967; Paczyński & Ziółkowski 1968; Han, Podsiadlowski & Eggleton 1994; Harpaz 1998). Recombination has since been studied in common-envelope (CE) evolution (Han, Podsiadlowski & Eggleton 1995), where the envelope of an evolved giant star expands and cools after interacting with an engulfed stellar companion. Sufficiently cooled layers of the envelope recombine, releasing energy that may further inflate the CE and aid in its ejection.

There have been observational suggestions that recombination energy may help eject CEs, based on reconstructing the CE parameters of wide post-CE binaries (Webbink 2008; Zorotovic et al. 2010; Davis, Kolb & Knigge 2012; Rebassa-Mansergas et al. 2012; Iaconi & De Marco 2019). Some population synthesis studies also find that models with large CE efficiency parameters ($\alpha_{\rm CE}$), which imply additional energy sources beyond orbital energy, such as recombination, are required to match the period distributions of e.g. subdwarf B stars (Han et al. 2003) and double white dwarfs (Nelemans et al. 2000). The role of recombination energy in CE evolution has been studied using 3D hydrodynamical simulations, 1D simulations, and analytical arguments based on (often) static, 1D stellar models.

Hydrodynamical simulations typically explore the additional amount of envelope mass that may be ejected when recombination energy is included and assumed to fully thermalize in the envelope. The latter assumption arises from the adiabatic nature of these simulations; simulating CE evolution in 3D with radiation hydrodynamics remains computationally challenging (but see Ricker et al. 2019). Whereas standard 3D CE simulations that do not model recombination typically result in ejecting few tens of per cent of the envelope (but see Law-Smith et al. 2020, who focused on the last 1 per cent of the dynamical plunge), including recombination energy has resulted in possible complete ejection (e.g. Nandez, Ivanova & Lombardi 2015; Ivanova & Nandez 2016; Reichardt et al. 2020; Sand et al. 2020; González-Bolívar et al. 2022; Lau et al. 2022). Some of these studies also found that most of the helium recombination energy may be used to expand the envelope, whereas a significant fraction of hydrogen recombination energy is released in material that has already become unbound. The effect of recombination energy on the final orbital separation is less clear. Both Ivanova & Nandez (2016) and Reichardt et al. (2020) compared CE simulations that include recombination energy with simulations that exclude it, reporting little difference in the final orbital separation. However, Sand et al. (2020) and González-Bolívar et al. (2022) both found a larger final separation when including recombination energy in CEs with asymptotic giant branch donors, despite these simulations also

★ E-mail: mike.lau@monash.edu

ejecting a larger fraction of the envelope mass. This was also reported by Lau et al. (2022) for a 12 $M_\odot$ red supergiant (RSG) donor, where including recombination energy resulted in a 20 per cent larger final separation.

However, interpreting these results requires caution, as the adiabatic assumption breaks down in the optically thin outer layers of the hydrogen partial ionization zone, where gas is allowed to cool radiatively. Hydrogen recombination radiation that is released in these regions may diffuse or stream away instead of driving expansion. More generally, including energy transport becomes important when simulating CE evolution past the dynamical spiral-in, and is essential for the self-regulated phase (Meyer & Meyer-Hofmeister 1979; Ivanova, Justham & Podsiadlowski 2015; Clayton et al. 2017). In 1D hydrodynamical simulations, radiation transport may be included, and convective energy transport may be treated using mixing length theory (e.g. Fragos et al. 2019, who use the dynamical module of MESA). However, caution is needed in discerning 1D artefacts, such as the effect of instantaneous energy homogenization in radial shells.

There have also been a number of analytical investigations based on static 1D stellar models that scrutinize the ability for recombination energy to aid in envelope ejection. One approach is based on comparing the expansion and energy transport time-scales in the envelope. With this approach, Sabach et al. (2017) estimated that convection should carry out half of the helium recombination energy to the photosphere, where it can be radiated away. Grichener, Sabach & Soker (2018) performed a similar analysis for an expanding envelope, claiming that most recombination energy is radiated away. Ivanova (2018) performed an analysis based on comparing the radiative, convective, and recombination energy fluxes, arguing instead that neither radiative diffusion nor convection may efficiently transport away hydrogen recombination energy released in bound layers of the envelope. Recently, Wilson & Nordhaus (2022) argue that convection is not efficient in carrying out the orbital energy injected by the companion in massive star CEs.

The combined efforts of 3D simulations, 1D simulations, and analytical arguments broadly converge on to several conclusions. First, recombination energy can be a significant energy source for envelope ejection if it is thermalized, although this can depend on the chosen boundary between the ejected envelope and the remaining bound mass, the so-called bifurcation point. Secondly, while helium recombination energy is injected in optically thick layers, the ability for hydrogen recombination energy to thermalize in the envelope is less certain. Despite this, there has not yet been a hydrodynamical simulation that studies the isolated role of helium recombination in the absence of hydrogen recombination, which would serve as a useful lower limit to the role of recombination energy.

In this work, we perform and compare simulations that include different recombination energy sources: (i) helium and hydrogen recombination (including molecular recombination to H_2), (ii) helium and hydrogen atomic recombination only, (iii) helium recombination only, and (iv) no recombination. Since our simulations are adiabatic, they implicitly assume recombination radiation is locally thermalized. By comparing (ii) and (iii), we disentangle the effects of hydrogen and helium recombination in a CE. This is difficult in past studies, which have only compared simulations including full recombination and without any recombination [i.e. comparing (i) and (iv) in our designation]. In those simulations, it is unclear whether a partially ionized layer that becomes unbound would have eventually been ejected through hydrodynamical interactions even in the absence of hydrogen recombination energy.

This paper is organized as follows. We summarize our set-up in Section 2 and explain our treatment of recombination in Section 3. In Section 4, we compare the fraction of unbound envelope mass (Section 4.1) and final separation (Section 4.2) between our simulations. In Section 5, we discuss the effect of recombination on the ejecta structure (Section 5.1) and the ability for recombination energy to thermalize in the envelope (Section 5.2). We summarize our findings in Section 6.

2 METHODS

Our simulations have the same set-up as our previous work (Lau et al. 2022, Paper I), except for a new implementation of recombination physics (see Section 3). In this section, we therefore summarize our set-up, and refer the reader to section 2 of Lau et al. (2022) for details.

We simulate a CE experienced by a 12 $M_\odot$ RSG donor with a 3 $M_\odot$ companion, using the same donor density profile as in Lau et al. (2022). We use a newer version of the smoothed particle hydrodynamics (SPH) code PHANTOM (v2022.0.1; Price et al. 2018), where we have introduced the ability to simulate fluids with non-uniform composition and a new equation of state (EoS) prescription that allows different recombination energy sources to be included separately (see Section 3). We resolve the donor star with 2×10^6 SPH particles, which was our default in Lau et al. (2022). We check convergence by comparison with a set of simulations carried out at lower resolution (using 2×10^5 SPH particles).

We set-up an initially circular orbit with separation 988 $R_\odot$, such that the donor's radius (618 $R_\odot$) exceeds its Roche radius by 30 per cent. The donor star is initially non-rotating, and we do not account for the effects of tidal distortion and thermal time-scale mass transfer, which are likely to modify the donor stellar profile during the onset of Roche lobe overflow. Lau et al. (2022) demonstrated that the donor star maintains its original density structure for at least 90 times the surface free-fall time when simulated in the absence of a companion.

We perform our simulations on the 64-core AMD EPYC 7742 Rome processors on the Flatiron Institute Rusty computing cluster, and on the 64-core Intel Xeon Platinum 8358 Icelake processors on the Flatiron Popeye computing cluster. A single CE simulation, using OpenMP parallelization, consumes roughly 100 kcpu-h, and requires 2 to 3 months of wall time. Our simulations conserve energy to within 0.04 per cent and angular momentum to within 0.02 per cent, due to our use of a single, global time-step for all particles.

3 TREATMENT OF RECOMBINATION

Atomic and molecular recombination are associated with an increase in mean molecular weight and, when in local thermodynamic equilibrium (LTE), an increase in thermal energy. These effects may be incorporated during EoS evaluation in a hydrodynamics code. In particular, the ionization potential manifests as an additional internal energy term. In our previous simulations that include recombination, we used the MESA EoS tables (Paxton et al. 2011, 2013, 2015, 2018, 2019), which are constructed from the OPAL EoS (Rogers, Swenson & Iglesias 1996; Rogers & Nayfonov 2002) and SCVH EoS (Saumon, Chabrier & van Horn 1995). This tabulated EoS includes the recombination energy available to various ionization states. For a typical stellar composition, the most significant sources are ionized and neutral hydrogen (forming H_2) and singly and doubly ionized helium. In order to separately investigate the effects of hydrogen and helium recombination, which is the aim of this paper, we instead

include the ionization potential, $\varepsilon_{\rm ion}$, of each species analytically in the expression for specific internal energy, u:

$$u = \frac{3k_{\rm B}T}{2\mu(x_i)m_{\rm u}} + \frac{a_{\rm rad}T^4}{\rho} + \varepsilon_{\rm ion}(x_i), \quad (1)$$

where ρ and T denote the gas density and temperature, and $k_{\rm B}$, $a_{\rm rad}$, and $m_{\rm u}$ are the Boltzmann constant, radiation constant, and atomic mass unit, respectively. μ is the mean molecular weight, which is a function of chemical composition (determined by the hydrogen and helium mass fractions, X and Y) and the ionization/dissociation fractions x_1,..., x_4 of H_2, H, He, and He^+, respectively. As the chemical composition is uniform in an RSG convective envelope, we assume fixed hydrogen and helium mass fractions, $X = 0.698$ and $Y = 0.287$, respectively.

The total specific recombination energy, or ionization potential, is a sum of its contribution from different hydrogen and helium ionization states,

$$\varepsilon_{\rm ion}(x_1, ..., x_4) = \varepsilon_{\rm H_2}x_1 + \varepsilon_{\rm H}x_2 + \varepsilon_{\rm He}x_3 + \varepsilon_{\rm He^+}x_4, \quad (2)$$

where, from left to right, the terms on the RHS are the specific recombination energies available to H (forming H_2), H^+, He^+, and He^{2+}.

The ionization potential of a given species depends on its ionization fraction, which, in LTE, depends on ρ and T via the Saha equations. Instead of solving Saha equations, we use accurate analytical fits of $x_i(\rho, T)$ to the MESA EoS table (Paxton et al. 2011, 2013, 2015, 2018, 2019) to ensure fast computational evaluation. The analytical expressions and fitting coefficients are provided in appendix C of Hirai et al. (2020). Each EoS evaluation involves solving for T in equation (1). This poses a challenge for traditional root finders like the Newton–Raphson method, which tends to diverge near the inflection points in $\varepsilon_{\rm ion}$ unless the initial guess is close to the solution. Our implementation uses the novel W4 method (Okawa et al. 2022) that shows better global convergence than Newton–Raphson-based methods.

To exclude a source of recombination energy, we remove its contribution from equation (2). In total, we compare simulations with five different implementations of recombination:

(i) 'He + H + H_2': We include the recombination energy of helium and hydrogen, including the energy released during H_2 molecular formation. All terms in equation (2) are retained.
(ii) 'He + H': We exclude the energy contributed by H_2 formation, including only the last three terms in equation (2).
(iii) 'He': We only include helium recombination energy (from both the singly and doubly ionized states), retaining only the last two terms in equation (2).
(iv) 'None': We do not allow any recombination energy to be deposited into the gas ($\varepsilon_{\rm ion} = 0$), but include the increase/decrease in mean molecular weight associated with recombination/ionization by retaining the dependence of $\mu = \mu(x_i)$ on the ionization fractions x_i.
(v) 'None, fixed μ': We neglect all effects of recombination, setting $\varepsilon_{\rm ion} = 0$ and fixing the mean molecular weight at $\mu = 0.62$, which corresponds to a fully ionized envelope with the same composition. This is identical to the 'gas + radiation' EoS simulation in Paper I (Lau et al. 2022).

3.1 The amount of available recombination energy

To obtain an upper limit to the role of recombination energy and understand the relative importance of different recombination energy sources, we plot in Fig. 1 the donor's binding energy profile when including different sources of recombination energy. We integrate the binding energy inwards from the surface as given by

$$E_{\rm bind}(>r) = \int_M^{m(r)} \left[\varepsilon_{\rm th}(m') + \varepsilon_{\rm ion}(m') - \frac{Gm'}{r'}\right] dm', \quad (3)$$

where $\varepsilon_{\rm th}$ is the thermal energy, $\varepsilon_{\rm ion}$ is the ionization potential from equation (2), and the third term in the integrand is the gravitational potential. The sum $u = \varepsilon_{\rm th} + \varepsilon_{\rm ion}$ is the specific internal energy, equivalent to equation (1). The vertical dashed line marks the location of our simulations' core boundary, $r_{\rm core} = 18.5\,{\rm R}_\odot$, which represents the base of the convective envelope. The value of $E_{\rm bind}(>r)$ at $r = r_{\rm core}$ is therefore the convective envelope's binding energy. The total gravitational binding energy is 1.2×10^{48} erg. If all of the envelope's thermal energy contributes to ejecting the envelope, the binding energy is reduced by more than a factor of 2, giving 5.1×10^{47} erg (the thermal energy for a gas-pressure dominated envelope is half the magnitude of the gravitational potential energy, and approaches the magnitude of the gravitational potential energy as radiation pressure becomes dominant).

The total ionization potential energy in the envelope is 2.5×10^{47} erg, of which 1.5×10^{47} erg (58 per cent) is from ionized hydrogen and 8.1×10^{46} erg (32 per cent) is from ionized helium. The contribution from the potential of H_2 formation, 2.4×10^{46} erg, is comparatively small (9.7 per cent). Applying the energy formalism, if recombination may be fully and efficiently used to eject the envelope, including helium recombination energy can increase the final separation by 16 per cent, while including both hydrogen and helium recombination can increase the final separation by 45 per cent, compared to if only thermal energy were fully used.

However, we note a number of ways by which the expectations outlined above are simplified. First, unlike thermal energy, recombination energy is released at specific temperatures: ≈6000 K

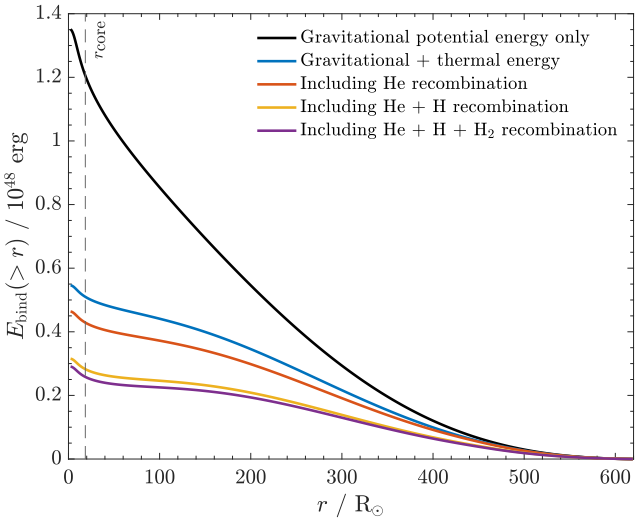

Figure 1. Comparison of the cumulative binding energy integrated from the surface (equation 3) when different sources of energy are included. The black line includes the gravitational potential energy only, while the blue line also includes thermal energy (first two terms of equation 1). The remaining lines successively include the following sources of recombination energy: helium recombination energy (red line), hydrogen atomic recombination energy (yellow line), and hydrogen molecular recombination energy (purple line). The vertical dashed line marks the location of the core boundary in our simulations.

Table 1. Summary of our simulation results, with those obtained at lower resolution in parentheses. From left to right, the columns list (i) the different recombination energy sources included in the simulation, as described in Section 3, (ii) the final separation, defined at a reference time when the ratio of the orbital period to the inspiral time-scale falls below a threshold ($-P_{\rm orb}\dot{a}/a < 5 \times 10^{-4}$). Columns (iii) and (iv) report the fraction of unbound envelope mass at that same reference point, with $f_{\rm k+p}$ assuming a purely mechanical criterion for considering material to be unbound and $f_{\rm k+p+th}$ also including thermal energy (see Section 4).

(i) Model	(ii) $a_{\rm f}/{\rm R}_\odot$	(iii) $f_{\rm k+p+th}$	(iv) $f_{\rm k+p}$
'He + H + H_2'	44.8 (37.7)	0.62 (0.77)	0.43 (0.64)
'He + H'	44.7 (39.3)	0.56 (0.65)	0.37 (0.54)
'He'	44.7 (40.0)	0.40 (0.48)	0.31 (0.45)
'None'	38.6 (34.6)	0.30 (0.36)	0.25 (0.32)
'None, fixed μ'	37.2 (34.0)	0.29 (0.40)	0.25 (0.37)

for hydrogen recombination, 13 000 K for He II recombination, 40 000 K for He III recombination, and 1300 K for H_2 molecular formation. If the initial adiabatic expansion driven by orbital energy deposition does not sufficiently cool the envelope to a recombination temperature, the associated recombination energy will not be released. Even if recombination energy were released in the envelope, its role in ejecting the envelope depends on where and when this energy is injected. For example, recombination may lead to runaway ejection if the binding energy at the partial ionization zone is less than the recombination energy released there (Ivanova et al. 2015; Ivanova & Nandez 2016). Recombination may also induce unstable pulsations during the self-regulated phase that could eject the whole envelope (Clayton et al. 2017, although we only model the dynamical phase). Finally, the contribution of recombination energy to the envelope binding energy depends on the envelope bifurcation point, diminishing with a deeper boundary where the magnitude of the gravitational potential may greatly exceed the ionization potential (Kruckow et al. 2016).

4 RESULTS

We examine two key quantities that characterize the outcome of a CE simulation: the fraction of unbound envelope mass (Section 4.1) and the final separation (Section 4.2). We consider a gas parcel as unbound if it has positive energy, and either use a 'mechanical' criterion that sums the specific kinetic and gravitational potential energies ($e_{\rm k} + e_{\rm p} > 0$) or a 'thermal' criterion that also includes thermal energy ($e_{\rm k} + e_{\rm p} + e_{\rm th} > 0$), excluding recombination energy. Table 1 lists each simulation's final separation, $a_{\rm f}$, and fraction of unbound envelope mass calculated with the thermal ($f_{\rm k+p+th}$) and mechanical criteria ($f_{\rm k+p}$), defined at a reference time where the inspiral time-scale is much longer than the orbital period, $-P_{\rm orb}\dot{a}/a < 5 \times 10^{-4}$, where a is the semimajor axis and $P_{\rm orb}$ is the orbital period.

We primarily reference $f_{\rm k+p+th}$ in the ensuing discussion. Although this thermal criterion assumes that thermal energy is eventually fully converted into mechanical work, which is not guaranteed, it yields an amount of unbound envelope mass that is closer to its asymptotic value (see our discussion in Paper I, Lau et al. 2022). We plot the evolution of the fraction of unbound envelope mass and the core-companion separation as functions of a shifted time, $t - t_0$, since the companion reaches 75 per cent of the initial donor radius (Figs 2 and 3).

4.1 Unbound envelope mass

Fig. 2 shows the evolution of the fraction of unbound envelope mass for the simulations listed in Section 3. For all simulations, material is still gradually becoming unbound at a rate of $\approx$0.1 $M_\odot$ yr^{-1} more than a decade after the dynamical plunge. Due to their large computational expense, we were unable to run the simulations long enough to find the final amount of unbound mass. Although the simulations at lower resolution (using 2×10^5 SPH particles) extend to $t - t_0 = 25$ yr. To compare the simulations, we therefore use the values of $f_{\rm k+p+th}$ in Table 1 as references, which are indicated with filled diamond markers in Fig. 2.

Excluding recombination energy ('None' and 'None, fixed μ') results in the smallest amount of ejected material ($f_{\rm k+p+th} = 0.30$ and $f_{\rm k+p+th} = 0.29$, respectively). On the other hand, both the 'He + H + H_2' and 'He + H' simulations eject at least 87 per cent of the envelope by the end ($f_{\rm k+p+th} = 0.62$ and 0.56, respectively), with the low-resolution results suggesting complete envelope ejection may be possible after another decade.

The simulation including only helium recombination energy ejects at least half of the envelope mass by the end, with $f_{\rm k+p+th} = 0.40$, which is 33 per cent larger than $f_{\rm k+p+th}$ for the simulation without recombination energy ('None'). On the other hand, comparing the 'He + H' and 'He' cases reveals that adding hydrogen recombination energy increases $f_{\rm k+p+th}$ by another 40 per cent, compared to the case where only helium recombination energy is included. This additional amount of unbound ejecta sets an upper bound on the role of hydrogen recombination for the simulated system, as our adiabatic simulations assume all recombination energy is locally thermalized. In reality, a significant fraction of hydrogen recombination energy may instead be radiated away, although we suggest in Section 5.2 that this may mainly occur in ejecta that are already unbound.

The fractions of unbound mass in the 'He + H + H_2' and 'He + H' simulations are very similar at any given time, implying H_2 formation plays an insignificant role in CE ejection. Their corresponding curves in Fig. 2 are almost identical up to $t - t_0 = 6$ yr after the plunge-in, because less than 1 per cent of the envelope mass in each case has cooled to temperatures conducive to H_2 recombination ($\approx$1300 K). But by the time ejecta can be adiabatically cooled to these temperatures, we find that they have already substantially expanded and become unbound. Even if the recombination energy of H_2 is injected into an envelope that is still bound, it constitutes less than 5 per cent of the envelope binding energy (see Section 3 and Fig. 1). Similarly, the role of dust-driven acceleration for CE ejection is expected to be insignificant in the system and time-scales we simulate. An upper limit may be obtained by assuming the initial stellar luminosity, $L \sim 10^{38}$ erg s^{-1}, is fully used to accelerate the entire envelope ($M_{\rm env} \sim 10^{34}$ g) over a duration $\Delta t \sim 100$ yr, taken to be much longer than the CE phase we simulate. The envelope velocity increases by $L\Delta t/(M_{\rm env}c) \sim 10^{-2}$ km s^{-1}, a negligible amount compared to the donor's surface escape velocity, $\approx$90 km s^{-1} (see also Glanz & Perets 2018, who focus on a 1 $M_\odot$ giant branch star and require $\Delta t = 1.3 \times 10^5$ yr to eject the envelope). While unimportant for envelope ejection, molecule and even dust formation may influence the formation of the surrounding nebula accelerated by winds from the stripped donor star in the post-CE binary (e.g. Pejcha, Metzger & Tomida 2016).

Comparing the 'None' and 'None, fixed μ' simulations allows us to isolate the effect of increased mean molecular weight, μ, associated with recombination. Fig. 2 shows that there are no significant differences in the fraction of unbound envelope mass, and

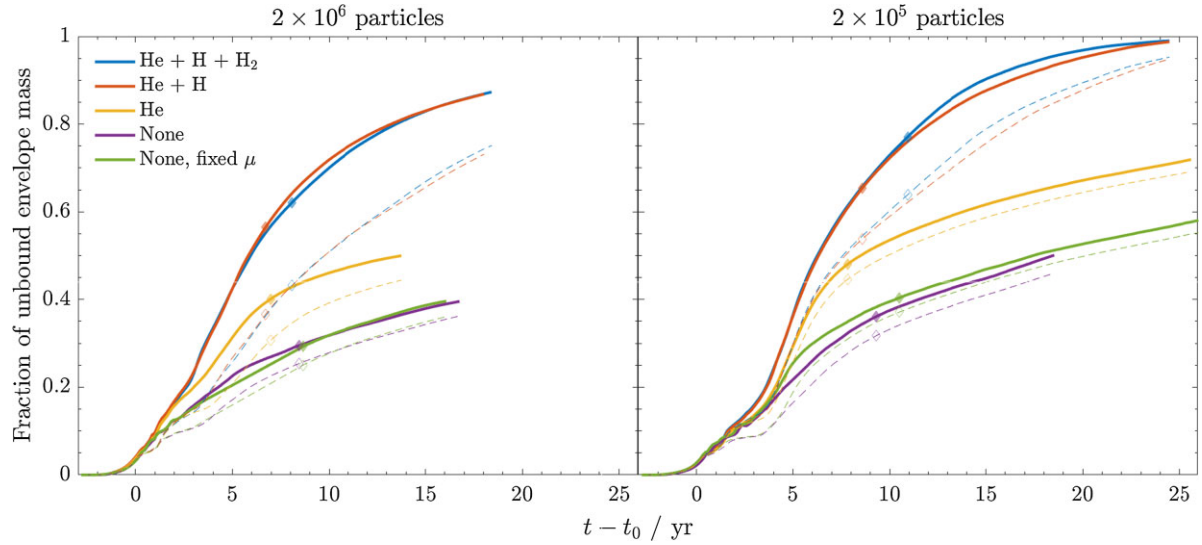

Figure 2. Comparison of the fraction of unbound envelope mass for simulations including different sources of recombination energy, as explained in Section 3. *Left-hand panel:* Results from our default simulations with 2×10^6 SPH particles. *Right-hand panel:* Results from simulations that use 10 times fewer SPH particles (2×10^5 particles), but are otherwise identical. The horizontal axis plots the time, $t - t_0$, since the companion plunges beneath 75 per cent of the initial donor radius. The diamond markers indicate where $-P_{\rm orb}\dot{a}/a$ falls beneath 5×10^{-4}, which is also the reference time we use to define a post-plunge-in semimajor axis, $a_{\rm f}$ (see Section 4.2). The solid lines consider a gas parcel as unbound if the sum of its kinetic, potential, and thermal energy is positive ($e_{\rm k} + e_{\rm p} + e_{\rm th} > 0$), while the dashed lines exclude thermal energy from the criterion (only requiring $e_{\rm k} + e_{\rm p} > 0$).

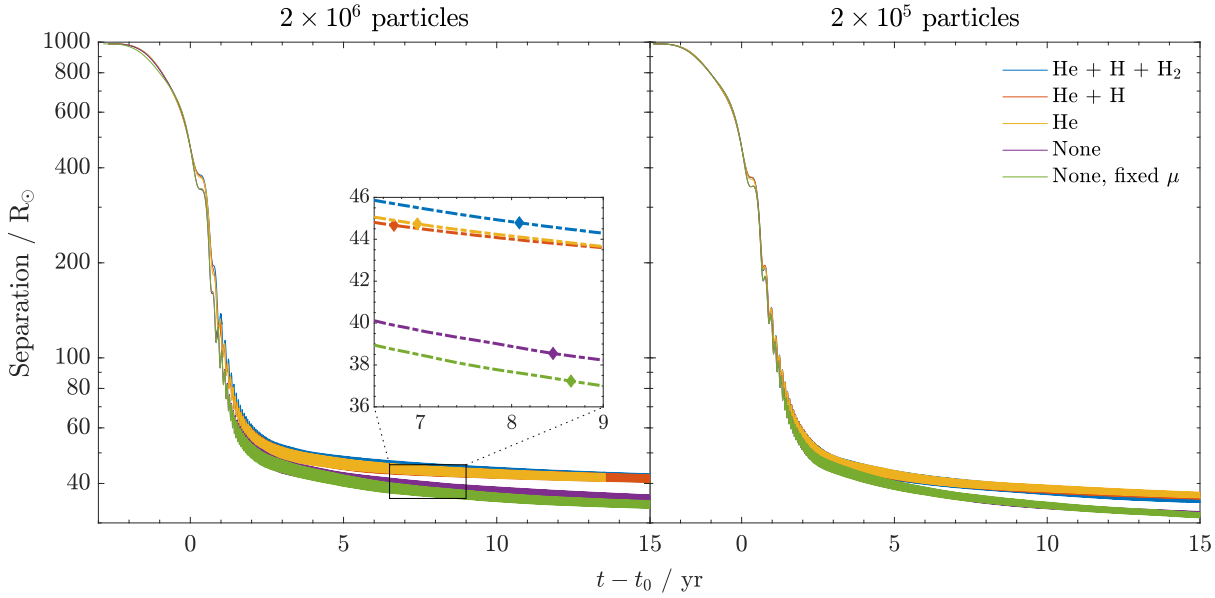

Figure 3. Same as Fig. 2, but instead showing the evolution in core-companion separation. In the left-hand panel, we show a magnified region between $t - t_0 = 6.5$ and 9.0 yr to highlight model differences. The magnified region shows the orbital semimajor axis, a, of the stellar cores instead of the instantaneous separation. The diamond markers indicate the orbital semimajor axis, $a_{\rm f}$, at which $-P_{\rm orb}\dot{a}/a$ falls beneath 5×10^{-4}.

so recombination mainly impacts the amount of unbound material via its energetic contribution.

Fig. 2 also reveals finite-resolution effects through comparison with simulations performed with 10 times fewer SPH particles, shown as the faded lines. At lower resolution, less material is ejected near the dynamical plunge-in ($t - t_0 \approx 0$), but more material is ejected during the slow spiral-in ($t - t_0 \gtrsim 3$). The first effect can be understood as follows. During the dynamical plunge-in, the energy injection mechanism is shock heating, where material becomes unbound after it is swept by the companion's bow shock one or more times. The shock front is more finely resolved and therefore heats gas in a more concentrated region with higher resolution, leading to a higher fraction of unbound SPH particles. The second effect is because the companion spirals in deeper during the plunge-in at lower resolutions (see Section 4.2 and Fig. 3). This results in relatively more energy injection (steeper increase in the frac-

tion of unbound envelope mass), seen near $3 \lesssim (t - t_0)/\,\mathrm{yr} \lesssim 6$ in Fig. 2.

The fraction of unbound envelope mass calculated with the purely mechanical ($e_\mathrm{k} + e_\mathrm{p} > 0$) criterion (dashed lines) is ≈5–20 per cent smaller than that calculated with our default criterion including thermal energy ($e_\mathrm{k} + e_\mathrm{p} + e_\mathrm{th} > 0$) (solid lines), which is similar to Moreno et al. (2022). We also observe that the discrepancy in the amount of unbound mass calculated with the two criteria is greater at higher resolution, indicating that the envelope's thermal to kinetic energy ratio is resolution dependent. This may be because that at higher resolution, more energy is stored as thermal energy in the convective eddies during the slow spiral-in (see Section 5.1). At lower resolutions, where these flows are less well resolved, orbital energy is more readily converted into kinetic energy.

4.2 Final separation

Fig. 3 shows that the rates of orbital shrinkage during the dynamical plunge are similar across different simulations, shrinking the orbit to ≈40−60 $\mathrm{R}_\odot$ within 3 yr. In our simulations, the orbital semimajor axis of the stellar cores continues to decrease gradually by a few times 0.1 $\mathrm{R}_\odot\ \mathrm{yr}^{-1}$ even nearly a decade after the dynamical plunge-in. We therefore define the final separation, a_f, at a reference time where the inspiral time-scale becomes 2000 times longer than the orbital period, $-P_\mathrm{orb}\dot{a}/a < 5 \times 10^{-4}$. The final separations, a_f, of all our simulations are listed in Table 1.

These separations, along with the magnified region shown in Fig. 3, show that the final separations for the five different models cluster around two distinct values. The simulations that include at least one source of recombination energy ('He + H + H_2', 'He + H', and 'He') have similar final separations ($a_\mathrm{f} = 44.7$−$44.8\,\mathrm{R}_\odot$) that are approximately 16 per cent higher than models that do not ('None' and 'None, fixed μ', with $a_\mathrm{f} = 38.6$ and 37.2 $\mathrm{R}_\odot$, respectively).

The larger final separations in CE simulations performed with recombination energy is consistent with a number of previous studies (Sand et al. 2020; González-Bolívar et al. 2022; Lau et al. 2022), supporting the idea that the additional envelope expansion driven by recombination energy helps stall the dynamical plunge-in earlier. However, these studies did not distinguish the effects of different recombination energy sources. Our results suggest helium recombination rather than hydrogen recombination as the main cause of the larger final separation. This can be inferred from the fact that the addition of hydrogen recombination energy in the 'He + H' simulation, despite ejecting 40 per cent more material relative to the 'He' simulation, does not halt the dynamical plunge-in earlier. The 'He + H' and 'He' simulations have similar final separations, $a_\mathrm{f} = 44.7\,\mathrm{R}_\odot$ in both cases. This could be because most of the hydrogen recombination energy is injected after the plunge-in and in the outer, marginally bound parts of the CE that are energetically decoupled from the inner binary (Nandez & Ivanova 2016). Helium recombination, however, occurs much deeper in the CE, where most of the orbital energy is released. On the other hand, Ivanova & Nandez (2016) and Reichardt et al. (2020) do not find that recombination energy changes the final separation significantly in their simulations. These varying findings in the literature are conceivably due to differences in starting models. For example, donor stars with different masses and at different evolutionary stages have partial ionization zones located at different relative mass coordinates.

The 'He + H + H_2' and 'He + H' simulations have similar final separations ($a_\mathrm{f} = 44.8$ and 44.7 $\mathrm{R}_\odot$, respectively), consistent with our finding in Section 4.1 that H_2 formation plays an insignificant role.

The simulations conducted with 10 times fewer SPH particles have final separations that are around 10 per cent smaller (Fig. 3, right-hand panel). However, the relative differences between each simulation are consistent with our discussion above for the default simulations. Particularly, the finding that helium recombination energy increases a_f, as opposed to hydrogen recombination energy, still holds.

5 DISCUSSION

5.1 Impact of recombination on the ejecta

We compare the impact of different types of recombination on the ejecta structure and morphology. Figs 4 and 5 show temperature slices of the CE across different simulations at $t = 9.97$ yr (around $t - t_0 = 7.3$ yr, depending on the simulation). The ejecta form an asymmetric structure consisting of hot, low-density bipolar cocoons expanding at ≈10−15 $\mathrm{km\,s}^{-1}$. As seen from the edge-on slices shown in Fig. 5, these lobes are around $10^4\,\mathrm{R}_\odot$ in extent, and enshrouded in unbound material that was ejected prior to the plunge-in (see also MacLeod, Ostriker & Stone 2018; Ondratschek et al. 2022). These cocoons are driven by 100–120 $\mathrm{km\,s}^{-1}$ outflows launched near the stellar cores, perpendicular to the orbital plane. These outflows are hydrodynamically collimated by comparatively dense and hot, bound material in the equatorial region that are about $\sim 10^3\,\mathrm{R}_\odot$ in radius. Convective mixing develops in this bound material, as shown in the orbital plane slices in Fig. 4. The formation of bipolar outflows is qualitatively consistent with observations of post-CE nebulae (e.g. Kamiński et al. 2018), but a proper comparison would require modelling the expansion of the nebula driven by irradiation and stellar winds from the stripped core (Frank et al. 2018; García-Segura, Ricker & Taam 2018; Zou et al. 2020).

In Figs 4 and 5, there are visible differences between the upper and the lower panels. The simulations in the upper panels include hydrogen recombination energy, which causes the coolest material to expand past $\approx 2 \times 10^4\,\mathrm{R}_\odot$ from the centre, and yet also retain higher temperatures (though the temperatures remain unrealistically high in our simulations due to the absence of radiative cooling, which should be particularly efficient after hydrogen recombination). The white line is a contour of constant hydrogen ionization fraction, $1 - [\mathrm{H\,I}] = 0.7$, which we show in Section 5.2 encloses the region where most useful recombination energy is injected. This contour is more spherical and uniform in temperature [at the recombination temperature $\log(T\ /\ \mathrm{K}) \approx 3.8$], and encloses a larger region than in the lower panels. We ascertain that this is a result of hydrogen recombination energy, rather than orbital energy injected by the stellar cores, from observing that the temperature slices of the 'He' simulation look qualitatively different from those of the 'He + H' simulation, despite having nearly the same final separations.

The 'He' and 'None' simulations are similar to each other, both displaying stronger convective mixing, leading to greater temperature inhomogeneity in the ejecta. Convection in the bound ejecta is induced by gradual heating by the slowly in-spiralling stellar cores after the dynamical phase (Lau et al. 2022; Moreno et al. 2022). The greater amount of bound and infalling material in the 'He' and 'None' cases could contribute to the more prominent mixing. There also appears to be slightly more convective plumes in the 'None' case, which could be due to the ≈16 per cent smaller final separation of the stellar cores, which must have injected more energy to the surrounding medium.

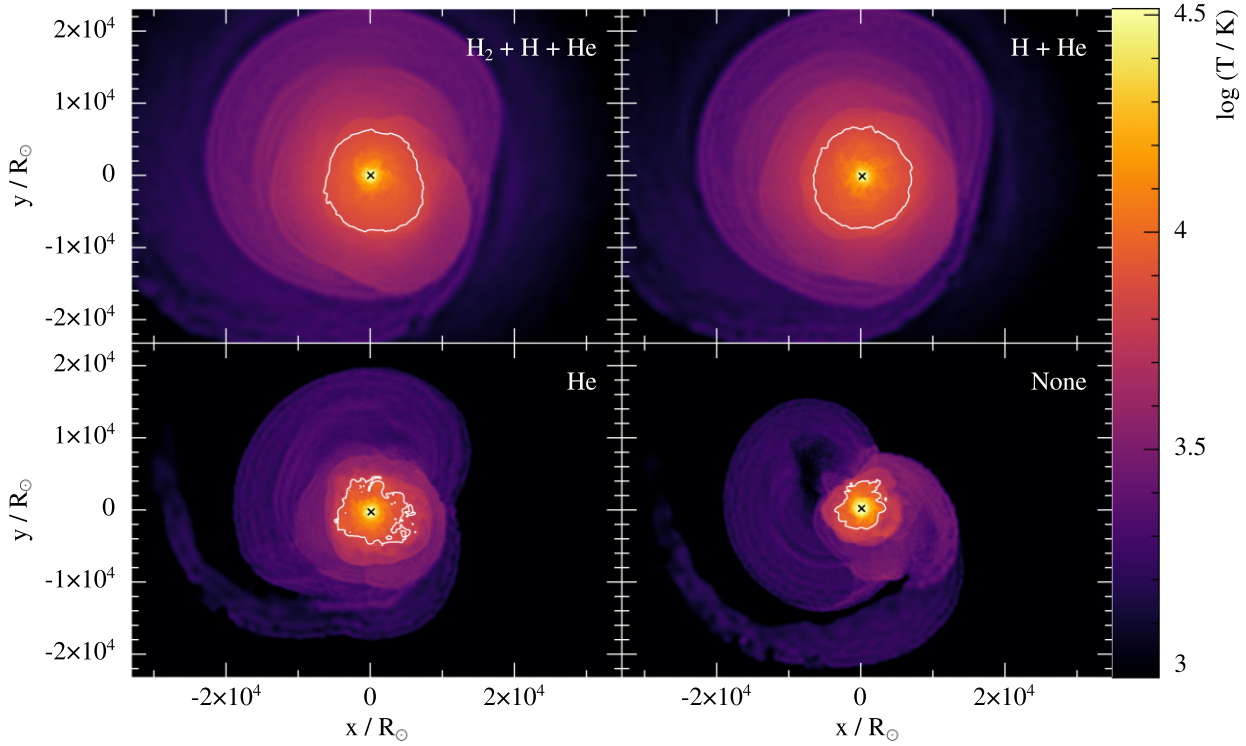

Figure 4. Comparison of the ejecta temperature in the $z = 0$ (face-on) cross-section across the various simulations at $t = 9.97$ yr, showing more expanded and uniform-temperature ejecta where hydrogen recombination has been included (simulations in the top panels). The white line is a contour of constant hydrogen ionization fraction, $1 - [\mathrm{H\,I}] = 0.7$, indicating where hydrogen recombination is actively occurring. The black crosses indicate the locations of the stellar cores. All simulation renderings in this paper were created with SPLASH (Price 2007). Videos of our simulations are available at https://themikelau.github.io/CE_recombination.

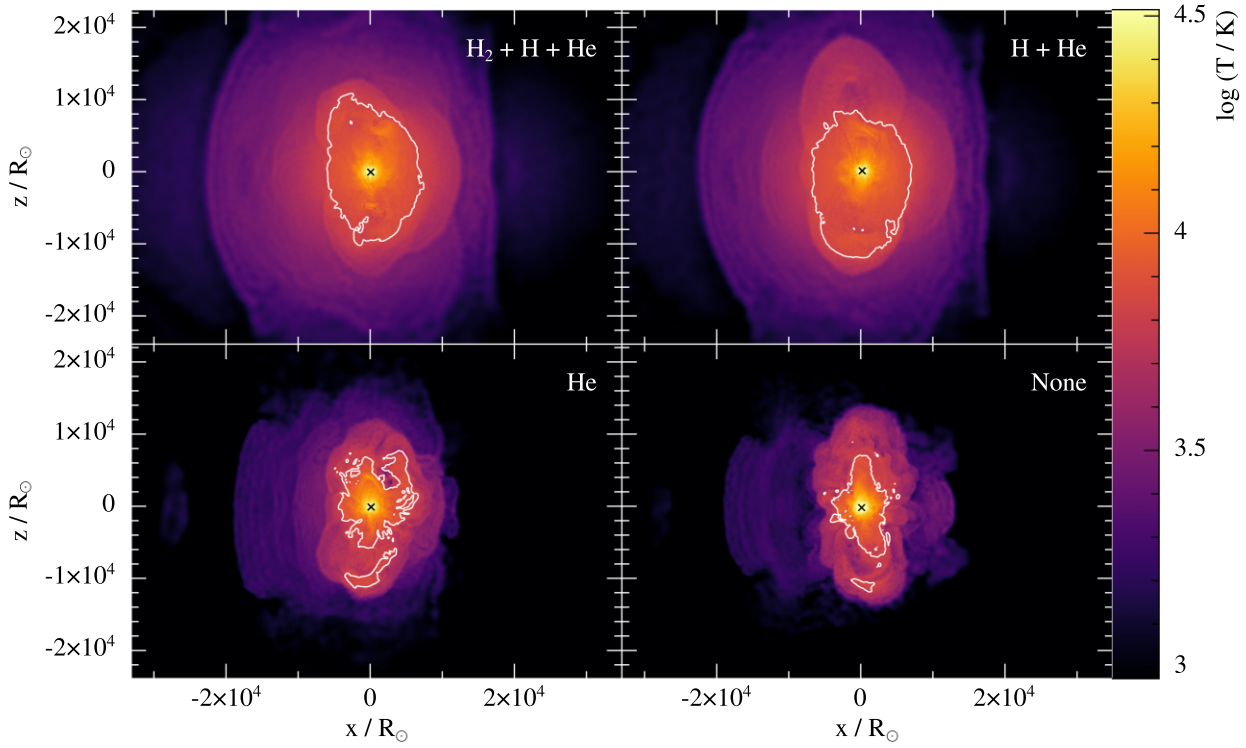

Figure 5. Same as Fig. 4, but showing the $y = 0$ (edge-on) cross-section.

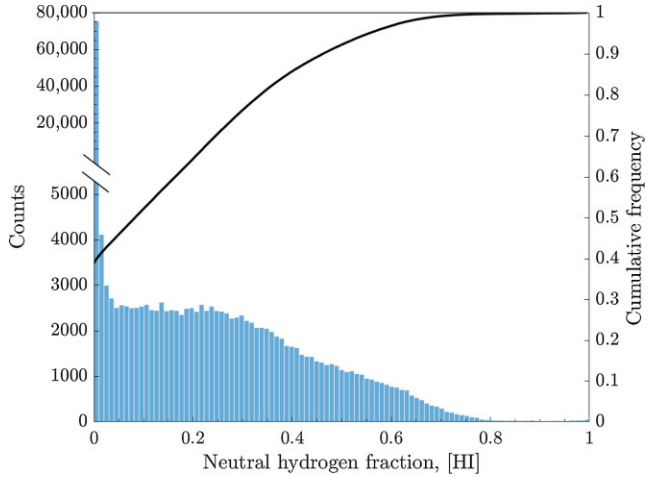

Figure 6. Histogram of the neutral hydrogen fraction, [H I], of SPH particles at the moment they are marked as unbound (attaining positive energies). The black line shows the cumulative frequency. We break the left vertical axis between 6000 and 10 000 counts to accommodate for the large amount of material ejected while hydrogen is still fully ionized.

5.2 The ability for recombination energy to thermalize

Thermal energy injected by the plunging companion's bow shock or by recombination can either perform work to expand the envelope or be transported away by processes such as radiation and convection, in the absence of other heat sources and sinks. Our adiabatic simulations might overestimate the amount of work done on the envelope by these processes as there is no radiation transport. A number of existing works estimate the ability for recombination energy to expand the CE (Sabach et al. 2017; Grichener et al. 2018; Ivanova 2018; Soker, Grichener & Sabach 2018), which is a matter of ongoing discussion. Wilson & Nordhaus (2019, 2020) have also suggested that the post-CE separation could be determined by the boundary at which convection is able to transport away the luminosity injected into the envelope during the dynamical plunge-in. More recently, their extension to CEs with massive stellar donors shows that the envelope expansion time-scale is short compared to the convective transport time-scale computed with static 1D stellar models (Wilson & Nordhaus 2022).

In our simulations, helium recombination occurs on the time-scale of the plunge-in, as the plunge-in directly drives the expansion of the envelope through the helium partial ionization zone. So if convective transport is unlikely to take away orbital energy, it is also unlikely to take away helium recombination energy. Helium recombination energy is also released in deep, optically thick layers of the CE, and so cannot be transported away by radiative diffusion. Our 'He' simulation, which finds a 16 per cent larger final separation and 33 per cent more ejected material, therefore likely represents a lower limit to the efficacy of recombination energy to help eject a CE for our chosen binary system.

On the other hand, the existing literature suggests hydrogen recombination energy to be less efficiently used, as a substantial portion is injected in optically thin layers, where it can be radiated away (Grichener et al. 2018). Yet, this does not directly imply that our adiabatic simulations overestimate the amount of ejected material, if the recombination energy that should have been radiated away is released in material that is already unbound. To see whether this is true, we plot in Fig. 6 the distribution of neutral hydrogen fraction, [H I], recorded at the moment when each SPH particle is marked as unbound according to our criterion.[1] We display results for the 'He + H' simulation conducted with 2×10^5 SPH particles, which completely ejects the envelope by the end of runtime. The counts across all bins therefore sum up to 2×10^5. The black line shows the normalized cumulative count. The distribution is dominated by a peak at [H I] = 0 (containing 38 per cent of the envelope mass), which includes all material that was ejected without any use of hydrogen recombination energy. The distribution is flat up to [H I] ≈ 0.3 (containing 80 per cent of the envelope mass), beyond which it linearly declines to [H I] ≈ 0.8. This shows that a relatively small fraction of the available hydrogen recombination energy (median of 0.085) produces the 40 per cent more unbound material seen in Fig. 2.

Previous works studying thermally expanding, 1D hydrostatic stellar models have shown that these largely ionized layers ([H I] $\lesssim$ 0.5) are sufficiently optically thick that photon diffusion is unlikely to prevent recombination energy from driving expansion (Grichener et al. 2018; Soker et al. 2018). The energy released at lower ionization fractions is not responsible for the additional amount of ejected material in the 'He + H' simulations, and would instead contribute to the H α emission of luminous red novae associated with CEs (Ivanova et al. 2013; MacLeod et al. 2017; Matsumoto & Metzger 2022). Grichener et al. (2018) instead suggest that convective transport might be efficient in transporting away hydrogen recombination energy in more ionized layers. However, this hydrogen partial ionization zone is marginally unbound, outflowing at significant fractions of the sound speed, and significantly out of hydrostatic equilibrium, and so departs from the regime of applicability of mixing length theory. Convective transport is therefore expected to be much less efficient than in a 1D hydrostatic profile. It would be valuable to self-consistently model convection in a CE by incorporating radiation transport into 3D simulations (see e.g. Ricker et al. 2019).

6 SUMMARY AND CONCLUSIONS

We studied the role of different sources of recombination energy in the CE evolution experienced by a massive star donor. We performed a series of 3D hydrodynamical simulations involving a 12 $M_\odot$ RSG donor with a 3 $M_\odot$ companion, using the set-up from our previous work (Lau et al. 2022). These simulations include different sources of recombination energy, assumed to thermalize locally in the envelope. By comparing these simulations, we have been able to infer the distinct effects of hydrogen and helium recombination. We list our main findings as follows:

(i) Helium recombination energy, comprising 32 per cent of the envelope's total recombination energy, leads to ejecting 33 per cent more envelope mass, compared to when recombination energy is not included at all. This energy is released deep in the envelope, where it is unlikely to be transported away by radiative diffusion or convection, and so represents a likely lower limit to the use of recombination energy in CE evolution.

(ii) Our simulations including both hydrogen and helium recombination eject at least 87 per cent of the envelope upon termination. Mass is still becoming unbound at a rate of $\approx 0.1\,M_\odot\ \mathrm{yr}^{-1}$. Simulations including hydrogen and helium recombination energy eject the

[1] It is possible for a particle to transition between states of negative and positive total energy more than once. In that case, we record the hydrogen ionization fraction during the particle's final transition from negative to positive total energy.

full envelope when evolved at lower resolution for another decade. Hydrogen recombination therefore leads to 40 per cent more ejected envelope mass compared to just including helium recombination energy.

(iii) Only a small fraction of hydrogen recombination energy is required to eject this additional unbound material. The majority (80 per cent) of the ejecta becomes unbound when only less than 30 per cent of the hydrogen recombination energy has been released. In these layers, which are more ionized and therefore more optically thick, a large fraction of recombination radiation is expected to thermalize in the envelope and radiative diffusion is inefficient.

(iv) Molecular recombination into H_2 plays an insignificant role in CE ejection, because almost all the material that is able to adiabatically cool to $\approx$1300 K is already unbound. The energy available from molecular recombination is also limited, comprising only 5 per cent of the envelope binding energy for our RSG donor.

(v) Helium recombination increases the final separation by $\approx$16 per cent. This is because helium recombination occurs deeper in the CE where most of the orbital energy is released, unlike hydrogen recombination. Adding hydrogen recombination does not significantly alter the final separation.

(vi) The ejecta in our simulations contain hot, low-density cocoons inflated by bipolar outflows. The deposition of hydrogen recombination energy results in more extended and spherically symmetric ejecta, and reduces the amount of convective mixing in the bound material near the stellar cores.

ACKNOWLEDGEMENTS

We thank Orsola De Marco and Miguel González-Bolívar for useful discussions. MYML acknowledges support by an Australian Government Research Training Program (RTP) Scholarship. IM is a recipient of the Australian Research Council Future Fellowship FT190100574. Parts of this research were supported by the Australian Research Council Centre of Excellence for Gravitational Wave Discovery (OzGrav), through project number CE170100004, and in part by the National Science Foundation under grant number NSF PHY-1748958. Parts of the simulations presented in this work were performed on the Rusty supercomputer and Popeye supercomputer of the Flatiron Institute, which is supported by Simons Foundation, on the Gadi supercomputer of the National Computational Infrastructure (NCI), which is supported by the Australian Government, and on the OzSTAR national facility at the Swinburne University of Technology. The OzSTAR program receives funding in part from the Astronomy National Collaborative Research Infrastructure Strategy (NCRIS) allocation provided by the Australian Government.

DATA AVAILABILITY

The data used to produce all figures in this article are available on Monash University's Bridges repository, at https://dx.doi.org/10.26180/20418837.v2.

REFERENCES

Clayton M., Podsiadlowski P., Ivanova N., Justham S., 2017, MNRAS, 470, 1788
Davis P. J., Kolb U., Knigge C., 2012, MNRAS, 419, 287
Fragos T., Andrews J. J., Ramirez-Ruiz E., Meynet G., Kalogera V., Taam R. E., Zezas A., 2019, ApJ, 883, L45
Frank A., Chen Z., Reichardt T., De Marco O., Blackman E., Nordhaus J., 2018, Galaxies, 6, 113
García-Segura G., Ricker P. M., Taam R. E., 2018, ApJ, 860, 19
Glanz H., Perets H. B., 2018, MNRAS, 478, L12
González-Bolívar M., De Marco O., Lau M. Y. M., Hirai R., Price D. J., 2022, MNRAS, preprint (arXiv:2205.09749)
Grichener A., Sabach E., Soker N., 2018, MNRAS, 478, 1818
Han Z., Podsiadlowski P., Eggleton P. P., 1994, MNRAS, 270, 121
Han Z., Podsiadlowski P., Eggleton P. P., 1995, MNRAS, 272, 800
Han Z., Podsiadlowski P., Maxted P. F. L., Marsh T. R., 2003, MNRAS, 341, 669
Harpaz A., 1998, ApJ, 498, 293
Hirai R., Sato T., Podsiadlowski P., Vigna-Gómez A., Mandel I., 2020, MNRAS, 499, 1154
Iaconi R., De Marco O., 2019, MNRAS, 490, 2550
Ivanova N., 2018, ApJ, 858, L24
Ivanova N., Nandez J. L. A., 2016, MNRAS, 462, 362
Ivanova N., Justham S., Avendano Nandez J. L., Lombardi J. C., 2013, Science, 339, 433
Ivanova N., Justham S., Podsiadlowski P., 2015, MNRAS, 447, 2181
Kamiński T., Steffen W., Tylenda R., Young K. H., Patel N. A., Menten K. M., 2018, A&A, 617, A129
Kruckow M. U., Tauris T. M., Langer N., Szécsi D., Marchant P., Podsiadlowski P., 2016, A&A, 596, A58
Lau M. Y. M., Hirai R., González-Bolívar M., Price D. J., De Marco O., Mandel I., 2022, MNRAS, 512, 5462
Law-Smith J. A. P. et al., 2020, preprint (arXiv:2011.06630)
Lucy L. B., 1967, AJ, 72, 813
MacLeod M., Macias P., Ramirez-Ruiz E., Grindlay J., Batta A., Montes G., 2017, ApJ, 835, 282
MacLeod M., Ostriker E. C., Stone J. M., 2018, ApJ, 868, 136
Matsumoto T., Metzger B. D., 2022, ApJ, 936, 114
Meyer F., Meyer-Hofmeister E., 1979, A&A, 78, 167
Moreno M. M., Schneider F. R. N., Roepke F. K., Ohlmann S. T., Pakmor R., Podsiadlowski P., Sand C., 2022, A&A, preprint (arXiv:2111.12112)
Nandez J. L. A., Ivanova N., 2016, MNRAS, 460, 3992
Nandez J. L. A., Ivanova N., Lombardi J. C. J., 2015, MNRAS, 450, L39
Nelemans G., Verbunt F., Yungelson L. R., Portegies Zwart S. F., 2000, A&A, 360, 1011
Okawa H., Fujisawa K., Yamamoto Y., Yasutake N., Ogata M., Yamada S., 2022, preprint (arXiv:2204.09941)
Ondratschek P. A., Röpke F. K., Schneider F. R. N., Fendt C., Sand C., Ohlmann S. T., Pakmor R., Springel V., 2022, A&A, 660, L8
Paczyński B., Ziółkowski J., 1968, Acta Astron., 18, 255
Paxton B., Bildsten L., Dotter A., Herwig F., Lesaffre P., Timmes F., 2011, ApJS, 192, 3
Paxton B. et al., 2013, ApJS, 208, 4
Paxton B. et al., 2015, ApJS, 220, 15
Paxton B. et al., 2018, ApJS, 234, 34
Paxton B. et al., 2019, ApJS, 243, 10
Pejcha O., Metzger B. D., Tomida K., 2016, MNRAS, 455, 4351
Price D. J., 2007, Publ. Astron. Soc. Aust., 24, 159
Price D. J. et al., 2018, Publ. Astron. Soc. Aust., 35, e031
Rebassa-Mansergas A. et al., 2012, MNRAS, 423, 320
Reichardt T. A., De Marco O., Iaconi R., Chamandy L., Price D. J., 2020, MNRAS, 494, 5333
Ricker P. M., Timmes F. X., Taam R. E., Webbink R. F., 2019, in Oskinova L. M., Bozzo E., Bulik T., Gies D. R., eds, Proc. IAU Symp. 346, High-mass X-ray Binaries: Illuminating the Passage from Massive Binaries to Merging Compact Objects. Cambridge Univ. Press, Cambridge, p. 449
Rogers F. J., Nayfonov A., 2002, ApJ, 576, 1064
Rogers F. J., Swenson F. J., Iglesias C. A., 1996, ApJ, 456, 902
Roxburgh I. W., 1967, Nature, 215, 838
Sabach E., Hillel S., Schreier R., Soker N., 2017, MNRAS, 472, 4361
Sand C., Ohlmann S. T., Schneider F. R. N., Pakmor R., Röpke F. K., 2020, A&A, 644, A60
Saumon D., Chabrier G., van Horn H. M., 1995, ApJS, 99, 713
Soker N., Grichener A., Sabach E., 2018, ApJ, 863, L14

Webbink R. F., 2008, in Milone E. F., Leahy D. A., Hobill D. W., eds, Astrophysics and Space Science Library, Vol. 352, Short-Period Binary Stars: Observations, Analyses, and Results. Springer-Verlag, Berlin, p. 233
Wilson E. C., Nordhaus J., 2019, MNRAS, 485, 4492
Wilson E. C., Nordhaus J., 2020, MNRAS, 497, 1895
Wilson E. C., Nordhaus J., 2022, MNRAS
Zorotovic M., Schreiber M. R., Gänsicke B. T., Nebot Gómez-Morán A., 2010, A&A, 520, A86
Zou Y. et al., 2020, MNRAS, 497, 2855

This paper has been typeset from a TEX/LATEX file prepared by the author.